Available online at www.sciencedirect.com
SCIENCE DIRECT®
Journal of Sound and Vibration 273 (2004) 585–606
JOURNAL OF SOUND AND VIBRATION
www.elsevier.com/locate/jsvi

Plane hydroelastic beam vibrations due to uniformly moving one axle vehicle

D. Fleischer[a], S.-K. Park[b,*]

[a] Deutsche Eisenbahn-Consulting GmbH, Munich, Germany
[b] Bridge Engineering Laboratory, Department of Civil Engineering, Sung Kyun Kwan University, 300 Chunchun-Dong, Jangan-Gu, Suwon, Kyounggi-Do 440-746, South Korea

Received 10 December 2001; accepted 7 May 2003

Abstract

The hydroelastic vibrations of a beam with rectangular cross-section is analyzed under the effect of an uniformly moving single axle vehicle using modal analysis and two-dimensional potential flow theory of the fluid neglecting the effect of surface waves aside the beam. For the special case of homogeneous beam resting on the surface of a water filled prismatic basin, the normal modes are determined considering surface waves in beam direction under the condition of compensating the volume of the enclosed fluid. The way to determine the vertical acceleration of the single axle vehicle is shown, which governs the response of the system. As analysis results the course of wheel load, the surface waves along the beam and the flow velocity distribution of the fluid is demonstrated for a continuous floating bridge under the passage of a rolling mass moving with uniform speed.

1. Introduction

The vibration analysis of elastic structures under the effect of crossing vehicles is one of the main items for the discipline of structural dynamics (see Ref. [1] with exhaustive sources). At first, Stokes [2] solved the dynamic problem of a rolling mass crossing an elastic single span beam by neglecting the beam mass and using numerical series for solving the differential equation of beam. Later, Zimmermann [3] found the exact mathematical solution of this problem. Moreover, analytical solutions are given by Schallenkamp [4] considering the beam mass, Marquard [5] modeling the vehicle by two masses connected with spring and Ryazanova [29], who determined

*Corresponding author.
E-mail address: psk@yurim.skku.ac.kr (S.-K. Park).

0022-460X/$ - see front matter © 2003 Elsevier Ltd. All rights reserved.
doi:10.1016/S0022-460X(03)00518-2

the vertical course of an accelerated single mass using integral equation. The comprehensive works of Schuetz [6] and Drosner [7] solved the problem of coupled bridge–vehicle interaction numerically considering also the unevenness of roadway as well as contact loosing wheels.

Pontoon bridges were used since antiquity to cross wide rivers [8,9]. One of the most well-known pontoon bridges of Europe is the double storey steel pontoon bridge in Istanbul spanning over the Bosporos, which was constructed in the beginning of the 20th century. In the USA, the floating concrete Bridge across Hood Canal [10], which was constructed in 1960, suffered severe damages during stormy weather in 1979 [11]. Floating bridges usually are designed either by applying the theory of beams on elastic foundation and neglecting hydrodynamic effects, or more realistically by considering hydrodynamic effects using hydrodynamic masses and dampers [12,13,28] as well as strip theory [14]. Strip theory means dividing the floating structure into slices transverse to its longitudinal direction with plane flow along each slice. The effect of flow in longitudinal direction of the structure can be considered only approximately (Lewis-factor) and is of minor significance compared with the transverse flow due to waves and gusty winds, if the pontoon width or wavelength of surface waves is small compared with the distance of structural vibration nodes [15]. Based on this theory, for instance vibrations of pontoon bridges due to wave excitation were analyzed using finite element method (FEM) [15–17]. In case of traffic loaded lightweight pontoon bridges, like for instance military pontoon bridges, the flow in longitudinal bridge direction cannot be neglected caused by gravity waves running parallel with the structure [18]. For instance runways on floating ice in arctic regions were analyzed by Chonan [19] and Sneyd et al. [20–22] using the model of hydroelastic floating slab with infinite extension under the effect of running constant forces and solving the problem by the application of integral transforms.

Many investigations exist on the analysis of unforced hydroelastic structural vibrations. One of the first was Lamb [23], who determined the first and second coupled mode of a circular slab with water contact on one side applying Ritz method. Nowadays contributions are the analytical calculation of the coupled natural frequencies by Grim [24] for floating slabs spanning in one direction as well as by Bauer [25] for floating rectangular slabs and by Bauer/Eidel [26] for membrane spanning in one direction and floating on fluid filled rectangular tank. The dynamic differential equation of the floating structure was solved using Fourier series. The fluid was assumed frictionless and incompressible, except [19], and the fluid's behavior was described by linear potential theory, except [26].

In the following the linear theory of instationary hydroelastic vibrations will be applied on a homogeneous beam with rectangular cross-section under the effect of an uniformly moving single axle vehicle modeling traffic induced vibrations of a continuous pontoon bridge. For the coupled fluid–beam–vehicle problem two-dimensional flow parallel span and in depth direction will be considered. The problem will be solved analytically using modal analysis with Fourier series for the modes [27].

2. Problem

The floating beam to be investigated shall have homogeneous rectangular cross-section and fixed end supports allowing free end rotation; this is a suitable model for continuous floating

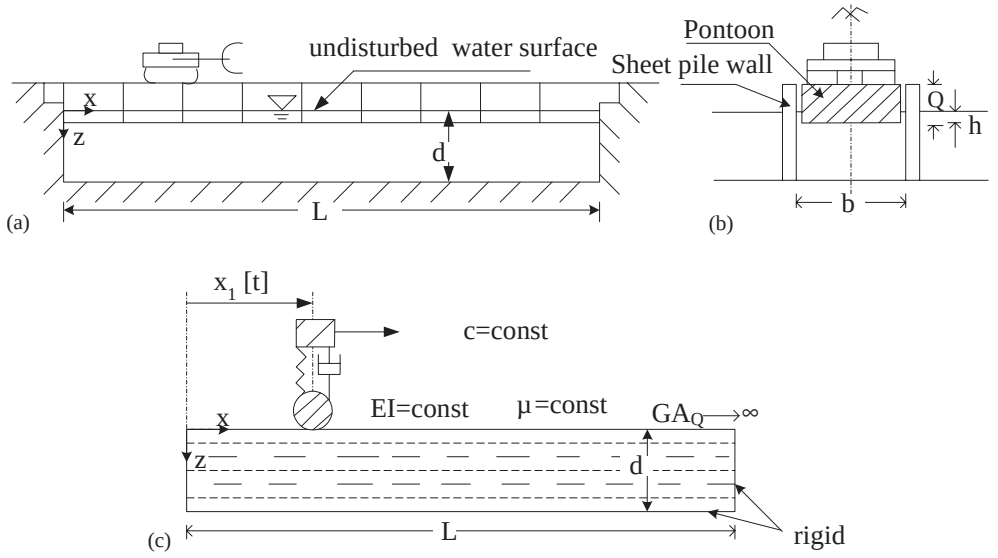

Fig. 1. System and load of the concerned floating bridge (a) longitudinal section, (b) cross-section, (c) model.

bridges with closely connected pontoons and ramps pressed to the banks. The riverbed shall have rectangular cross-section with rigid borderlines and shall contain still water (Fig. 1). The radiation of surface waves transverse to the beam bridge shall be neglected or shall be excluded by structural countermeasures like for instance rigid sheet piles or walls, so that plane water flow can be assumed along the beam in the fluid below.

The fluid is assumed incompressible and ideal one with non-rotational flow having the potential $\Phi(x, z, t)$, the local differentials of which are used to describe the flow velocity in each direction, and observing the physical law

$$\frac{\partial^2 \Phi}{\partial x^2} + \frac{\partial^2 \Phi}{\partial z^2} = 0. \tag{1}$$

The water pressure $p(x, z, t)$ within the fluid can be deducted from the in-stationary Bernoulli-equation

$$\frac{\partial \Phi}{\partial t} + \frac{v^2}{2} - gz + \frac{p - p_0}{\rho_F} = 0. \tag{2}$$

If the non-linear pressure $\rho_F v^2/2$ caused by the square of flow velocity v will be neglected, the following linear partial differential equation will describe the forced hydroelastic vibrations of the floating homogeneous Rayleigh-beam (see Appendix A):

$$\mu \frac{\partial^2 \tilde{w}(x,t)}{\partial t^2} - \rho I \frac{\partial^2}{\partial t^2}\left(\frac{\partial^2 \tilde{w}(x,t)}{\partial x^2}\right) + \rho_F g b \tilde{w}(x,t) - \rho_F b \frac{\partial \Phi(x,h,t)}{\partial t} + EI \frac{\partial^4 \tilde{w}(x,t)}{\partial x^4} + r_a \frac{\partial \tilde{w}(x,t)}{\partial t} + r_i I \frac{\partial}{\partial t}\left(\frac{\partial^4 \tilde{w}(x,t)}{\partial x^4}\right) = \delta(x - ct) P(t). \tag{3}$$

In this differential equation ρ is the density of the beam material, ρ_F is the density of the fluid, b is the beam width, I is the second moment of beam cross-section, E is the modulus of elasticity of

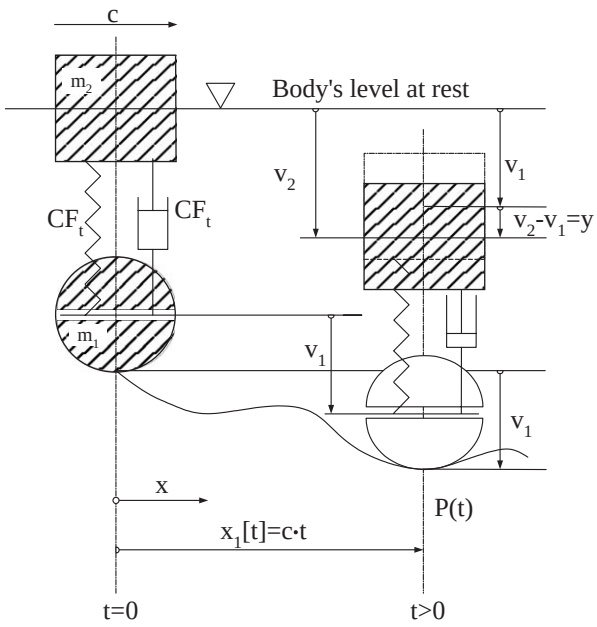

Fig. 2. Model and vertical displacements of vehicle on uneven track.

beam material, μ is the uniformly distributed beam mass, r_a is the environmental and r_i is the internal viscous damping constant of the beam and g is the gravity. Due to the lack of internal fluid friction and excluded lateral radiation of surface waves, there will occur no hydrodynamic damping, and only air as well as material damping will be effective. δ is the Dirac-function and $P(t)$ is the wheel load of the single axle vehicle running with uniform speed c along the centerline of the bridge according to Fig. 2. The dynamic deflection of the beam $\tilde{w}(x,t)$ describes the vibration around the static deflection of the beam $\bar{w}(x)$. The ordinate $z = h$ indicates the distance between the sub-surface of beam and the undisturbed water surface $z = 0$, and for simplicity can be assumed zero or equal to the static submerged depth of the beam.

The boundary conditions for the simple beam with free end-rotation are as follows:

$$\tilde{w}(0,t) = \tilde{w}(l,t) = 0, \quad \left.\frac{\partial^2 \tilde{w}(x,t)}{\partial x^2}\right|_{x=0} = \left.\frac{\partial^2 \tilde{w}(x,t)}{\partial x^2}\right|_{x=l} = 0 \tag{4}$$

and for the flow velocity of the fluid perpendicular to the borderlines of the rigid basin

$$\left.\frac{\partial \Phi}{\partial x}\right|_{x=0} = \left.\frac{\partial \Phi}{\partial x}\right|_{x=l} = \left.\frac{\partial \Phi}{\partial z}\right|_{z=d} = 0. \tag{5}$$

Along the sub-surface of the beam the vertical velocity of beam and fluid are the same, in other words, there the following compatibility condition must be met:

$$\left.\frac{\partial \Phi}{\partial z}\right|_{z=h} = \frac{\partial \tilde{w}}{\partial t}. \tag{6}$$

As the beam always shall be in contact with the enclosed fluid, the beam deflection line must meet the condition to compensate the displaced incompressible fluid volume as follows

(cf. Ref. [24]):

$$\int_0^l \tilde{w}(x,t)\,\mathrm{d}x = 0. \tag{7}$$

The wheel force of the single axle vehicle acting on track as shown in above Fig. 2 can be described according to Ref. [27] by

$$P(t) = c_0 + c_1 g_1(t) + c_2 g_2(t) - c_3 \ddot{v}_1(t) - \int_0^l \ddot{v}_1(t)[c_4 g_1(t-\tau) + c_5 g_2(t-\tau)]\,\mathrm{d}\tau \tag{8}$$

using expressions, which are explained in Appendix B.

3. Hydroelastic free vibrations

The differential equation describing free hydroelastic transverse vibration of the concerned beam can be derived from Eq. (3) without using the expressions for the damping and the external wheel force:

$$\mu \frac{\partial^2 \tilde{w}(x,t)}{\partial t^2} - \rho I \frac{\partial^2}{\partial t^2}\left(\frac{\partial^2 \tilde{w}(x,t)}{\partial x^2}\right) + \rho_F g b \tilde{w}(x,t) - \rho_F b \frac{\partial \Phi(x,h,t)}{\partial t} + EI \frac{\partial^4 \tilde{w}(x,t)}{\partial x^4} = 0. \tag{9}$$

The free vibration $\tilde{w}(x,t)$ of the beam and $\Phi(x,z,t)$ of the fluid must satisfy the boundary conditions (4)–(6) and condition (7) for compensating the displaced incompressible fluid volume.

The solution of the Laplace differential Eq. (1) is the potential

$$\Phi(x,z,t) = \mathrm{i}\omega \mathrm{e}^{\mathrm{i}\omega t} l^2 \bar{\Phi}(x,z) \tag{10}$$

with the dimensionless potential mode as Fourier-cosine series with period $2l$

$$\bar{\Phi}(x,z) = \frac{\bar{A}_0}{2} + \sum_{m=1}^{\infty} \bar{A}_m \frac{\cosh(m\pi d/l)(1-z/d)}{\cosh(m\pi d/l)} \cos(m\pi x/l). \tag{11}$$

Hereby, l is the beam length, ω is the natural circular frequency and $\mathrm{i} = \sqrt{-1}$. The constant factor $\mathrm{i}\omega l^2$ was used in order to get real Fourier coefficients (18a) and (26) when later satisfying the compatibility condition (6).

For the hydroelastic free vibration of the beam, the following separation approach will be applied:

$$\tilde{w}(x,t) = \mathrm{e}^{\mathrm{i}\omega t} l \psi_0(x/l)$$

with the definition of dimensionless mode function

$$\psi_0(x/l) := \bar{\psi}_0(x)$$

representing the deflection line of the hydroelastic free beam vibration. Based on above-mentioned approach and definition the deflection line of the hydroelastic free vibrating beam and its four differentials generally can be expressed by the formula

$$\frac{\partial^j \tilde{w}(x,t)}{\partial x^j} = \mathrm{e}^{\mathrm{i}\omega t} \frac{\bar{\psi}_j(x)}{l^{j-1}}, \quad j = 0,1,2,3,4 \tag{12a}$$

with $\bar{\psi}_j(x)$ as the dimensionless mode function of beam representing the jth local differential of the deflection line, defined as follows (the symbol ":=" means "definition")

$$\frac{\mathrm{d}\bar{\psi}_j(x)}{\mathrm{d}x} := \frac{1}{l}\bar{\psi}_{j+1}(x). \tag{12b}$$

In the following, the function $\bar{\psi}_0(x)$ will be called beam mode. Inserting the potential function (10) and the seperation approach (12a) into the differential equation of beam (9) will result in the homogeneous equation

$$(-\bar{\omega}^2 + \alpha_1)\bar{\psi}_0(x) + \alpha_3\bar{\omega}^2\bar{\psi}_2(x) + \alpha_2\bar{\omega}^2\bar{\Phi}(x,h) + \bar{\psi}_4(x) = 0 \tag{13}$$

with the square power of the dimensionless natural circular frequency

$$\bar{\omega}^2 := \frac{\omega^2\mu l^4}{EI} \tag{14a}$$

as eigenvalue and with the dimensionless parameters

$$\alpha_1 := \frac{\rho_F g b l^4}{EI}, \quad \alpha_2 := \frac{\rho_F b l}{\mu}, \quad \alpha_3 := \frac{\rho I}{\mu l^2} \tag{14b}$$

as coefficients representing the effect of elastic beam foundation (α_1), of hydrodynamics (α_2) and of beam gyration (α_3). Due to the symmetry of the system the vibrating beam will have antimetric (i.e., uneven) and symmetric (i.e., even) modes $\bar{\psi}_0(x)$. Antimetric beam modes automatically meet condition (7) for compensating the displaced incompressible fluid volume. If describing the antimetric beam modes by Fourier-sine series with period $2l$

$$\bar{\psi}_0(x) = \sum_{n=2,4,\ldots}^{\infty} \bar{W}_n^{(0)} \sin(n\pi x/l) \tag{15}$$

automatically the boundary conditions (4) of the beam are met. By differentiation of each term in series (15) we get the first four ($j = 1, 2, 3, 4$) dimensionless mode functions by differentiation of each term in series (15) observing definition (12b). Especially, the 2nd and 4th differential ($j = 2, 4$) is

$$\bar{\psi}_j(x) = \sum_{n=2,4,\ldots}^{\infty} \bar{W}_n^{(j)} \sin(n\pi x/l), \quad j = 2, 4 \tag{16}$$

with

$$\begin{aligned} \bar{W}_n^{(2)} &= -(n\pi)^2 \bar{W}_n^{(0)}, \quad n = 2, 4, \ldots, \\ \bar{W}_n^{(4)} &= (n\pi)^4 \bar{W}_n^{(0)}, \quad n = 2, 4, \ldots. \end{aligned} \tag{17}$$

Inserting the potential function (10) and the beam deflection (12a) ($j = 0$) into the compatibility condition (6), replacing the dimensionless modes by series (11) respectively (15), multiplying both sides with $2/l\cos(s\pi x/l)$, $s = 1, 2, \ldots$ and integrating each term of the series from $x = 0$ to l

we get

$$\bar{A}_m = -\frac{1}{m\pi}\frac{\cosh(m\pi d/l)}{\sinh(m\pi d/l)(1-h/d)}\sum_{n=2,4,\ldots}^{\infty}\bar{W}_n^{(0)}\alpha_{nm}, \quad \alpha_{nm} \coloneqq \frac{4}{\pi}\frac{n}{n^2-m^2} \quad \text{for} \quad m = 1,3,\ldots,$$
$$\bar{A}_m = 0 \quad \text{for } m = 2,4,\ldots. \tag{18a}$$

Obviously the potential function (11) is antimetric. Therefore, the constant of series (11) must disappear, i.e.,

$$\bar{A}_0 = 0. \tag{18b}$$

Inserting the Fourier-series (11), (15) and (16) into Eq. (13), multiplying both sides with $2/l\sin(s\pi x/l)$, $s = 2,4,\ldots$ and then integrating each term from $x = 0$ to $x = l$ results in the following general eigenproblem considering expressions (17) and (18a) for the Fourier-coefficients

$$([\mathbf{B}] - \lambda[\mathbf{A}])\mathbf{x} = 0, \quad = 1/\bar{\omega}^2 \tag{19}$$

with

$$\mathbf{x}^{\mathrm{T}} = (\bar{W}_2^{(0)}, \bar{W}_4^{(0)}, \ldots, \bar{W}_s^{(0)}, \ldots), \quad s = 2,4,\ldots \tag{20a}$$

and the coefficients of matrix [**A**]

$$a_{sn} = \begin{cases} \dfrac{\alpha_1}{s^4} + \pi^4 & \text{for } n = s, \\ 0 & \text{for } n \neq s \end{cases} \tag{20b}$$

as well as the coefficients of matrix [**B**]

$$b_{sn} = \frac{\alpha_2}{s^4}\sum_{m=1,3,\ldots}^{\infty}\frac{\coth(m\pi d/l)(1-h/d)}{m\pi}\alpha_{sm}\alpha_{nm} + \frac{1}{s^2}\begin{cases} \dfrac{1}{s^2} + \alpha_3\pi^2 & \text{for } n = s, \\ 0 & \text{for } n \neq s \end{cases} \tag{20c}$$

for $s = 2,4,\ldots$ and $n = 2,4,\ldots$ each.

Symmetric modes must be adjusted to condition (7) to compensate the displaced incompressible fluid volume. Using the Fourier-cosine series of period $2l$ to describe symmetric beam modes

$$\bar{\psi}_0(x) = \frac{\bar{B}_0^{(0)}}{2} + \sum_{n=2,4,\ldots}^{\infty}\bar{B}_n^{(0)}\cos(n\pi x/l) \tag{21}$$

this adjustment occurs by zero setting of the constant, i.e.,

$$\bar{B}_0^{(0)} = 0. \tag{22}$$

Moreover, the dimensionless mode functions for the four differentials of the beam deflection line also shall be expressed by Fourier-cosine series

$$\bar{\psi}_j(x) = \frac{\bar{B}_0^{(j)}}{2} + \sum_{n=1}^{\infty}\bar{B}_n^{(j)}\cos(n\pi x/l), \quad j = 1,2,3,4. \tag{23}$$

Based on the series for $\bar{\psi}_4(x)$ all Fourier coefficients can be expressed by the coefficients $\bar{B}_n^{(4)}$ using integration of each term and considering the boundary conditions (4). Especially, the Fourier coefficients for the symmetric beam mode ($j = 0$) and its second differential ($j = 2$) are as follows according to Ref. [27]:

$$\bar{B}_0^{(0)} = \frac{\bar{B}_0^{(4)}}{120} - \frac{2}{\pi^4} \sum_{n=2,4,\ldots}^{\infty} \frac{\bar{B}_n^{(4)}}{n^2} \left(\frac{\pi^2}{12} + \frac{1}{n^2} \right), \tag{24a}$$

$$\bar{B}_s^{(0)} = \begin{cases} -\dfrac{\bar{B}_0^{(4)}}{\pi^4 s^2} \left(\dfrac{\pi^2}{12} + \dfrac{1}{s^2} \right) + \dfrac{2}{\pi^4 s^2} \sum_{n=2,4,\ldots}^{\infty} \dfrac{\bar{B}_n^{(4)}}{n^2} + \dfrac{\bar{B}_s^{(4)}}{\pi^4 s^4}, & s = 2, 4, \ldots, \\ 0, & s = 1, 3, \ldots, \end{cases} \tag{24b}$$

$$\bar{B}_0^{(2)} = -\frac{\bar{B}_0^{(4)}}{12} + \frac{2}{\pi^2} \sum_{n=2,4,\ldots}^{\infty} \frac{\bar{B}_n^{(4)}}{n^2}, \tag{24c}$$

$$\bar{B}_s^{(2)} = \begin{cases} \dfrac{\bar{B}_0^{(4)}}{\pi^2 s^2} - \dfrac{\bar{B}_s^{(4)}}{\pi^2 s^2}, & s = 2, 4, \ldots, \\ 0, & s = 1, 3, \ldots. \end{cases} \tag{24d}$$

Inserting expression (24a) into condition (22) will give

$$\bar{B}_0^{(4)} = \frac{240}{\pi^4} \sum_{n=2,4,\ldots}^{\infty} \frac{\bar{B}_n^{(4)}}{n^2} \left(\frac{\pi^2}{12} + \frac{1}{n^2} \right). \tag{25}$$

Inserting the potential function (10) and the beam deflection line (12a) ($j = 0$) into the compatibility condition (6) as well as replacing the dimensionless modes by series (11) respectively (21) we get after comparison of coefficients

$$\bar{A}_m = \begin{cases} -\dfrac{\bar{B}_m^{(0)}}{m\pi} \dfrac{\cosh(m\pi d/l)}{\sinh(m\pi d/l)(1 - h/d)}, & m = 2, 4, \ldots, \\ 0, & m = 1, 3, \ldots, \end{cases} \tag{26}$$

i.e., the potential function (11) is symmetric.

Inserting the Fourier-series (11), (21) and (23) into Eq. (13), multiplying both sides with $2/l \cos(s\pi x/l)$, $s = 0, 2, 4, \ldots$ and finally integrating each term from $x = 0$ to l will give for $s = 0$ under consideration of expressions (22), (24c) and (25)

$$\bar{A}_0 = \frac{-2}{\pi^2 \alpha_2 \bar{\omega}^2} \sum_{n=2,4,\ldots}^{\infty} \frac{\bar{B}_n^{(4)}}{n^2} \left[\frac{120}{\pi^2} \left(\frac{\pi^2}{12} + \frac{1}{n^2} \right) \left(1 - \frac{\alpha_3 \bar{\omega}^2}{12} \right) + \alpha_3 \bar{\omega}^2 \right] \tag{27}$$

and for $s = 2, 4, \ldots$ under consideration of expressions (24b), (24d), (26) and (25) the general eigenproblem (19) with

$$\mathbf{x}^{\mathrm{T}} = (\bar{B}_2^{(4)}, \bar{B}_4^{(4)}, \ldots, \bar{B}_s^{(4)}, \ldots), \quad s = 2, 4, \ldots \tag{28a}$$

and the coefficients of matrix [**A**]

$$a_{sn} = \frac{2\alpha_1}{\pi^4 s^2 n^2}\left[\frac{-120}{\pi^4}\left(\frac{\pi^2}{12}+\frac{1}{s^2}\right)\left(\frac{\pi^2}{12}+\frac{1}{n^2}\right)+1\right] + \begin{cases} 1+\dfrac{\alpha_1}{\pi^4 s^4} & \text{for } n=s, \\ 0 & \text{for } n\neq s \end{cases} \tag{28b}$$

as well as the coefficients of matrix [**B**]

$$b_{sn} = \frac{2}{\pi^4 s^2 n^2}\left[\frac{-120}{\pi^4}\left(\frac{\pi^2}{12}+\frac{1}{s^2}\right)\left(\frac{\pi^2}{12}+\frac{1}{n^2}\right)+1\right]\left[1+\alpha_2\frac{\coth\dfrac{s\pi d}{l}\left(1-\dfrac{h}{d}\right)}{s\pi}\right]$$
$$-\frac{240\alpha_3}{\pi^6 s^2 n^2}\left(\frac{\pi^2}{12}+\frac{1}{n^2}\right)+\begin{cases} \dfrac{1}{\pi^4 s^4}\left[1+\alpha_2\dfrac{\coth\dfrac{s\pi d}{l}\left(1-\dfrac{h}{d}\right)}{s\pi}\right]+\dfrac{\alpha_3}{\pi^2 s^2} & \text{for } n=s, \\ 0 & \text{for } n\neq s \end{cases} \tag{28c}$$

for $s = 2, 4, \ldots$ and $n = 2, 4, \ldots$ each. The Fourier coefficients of the symmetric beam modes (21) can be calculated using Eq. (24b). In order to exactly meet the boundary conditions (4), the symmetric beam modes $\bar{\psi}_0(x)$ shall be re-calculated into Fourier-sine series resulting in

$$\bar{\psi}_0(x) = \sum_{n=1,3,\ldots}^{\infty} \bar{W}_n^{(0)} \sin(n\pi x/l) \tag{29}$$

with

$$\bar{W}_n^{(0)} = \sum_{s=2,4,\ldots}^{\infty} \bar{B}_s^{(0)} \alpha_{ns}, \quad n = 1, 3, \ldots,$$
$$\alpha_{ns} := \frac{4}{\pi}\frac{n}{n^2 - s^2}, \quad n = 1, 3, \ldots; \quad s = 2, 4, \ldots. \tag{30}$$

For the general eigenproblem (19) with eigenvector (20a) respectively (28a) an infinite number $p = 1, 2, \ldots$ of hydroelastic beam modes $\bar{\psi}_{0p}(x)$ and related natural circular frequencies $\bar{\omega}_p$ exist.

For example the hydroelastic free vibrations of a continuous floating bridge shall be investigated with parameters as follows:

$$\alpha_1 = 371160.7180, \quad \alpha_2 = 832.9910, \quad \alpha_3 = 1.2023 \times 10^{-7},$$
$$a_8 := d/l = 1.8667 \times 10^{-2}, \quad a_9 := h/d = \frac{1}{\alpha_2 \alpha_8} = 6.4312 \times 10^{-2}. \tag{31}$$

Fig. 3 shows the first four beam modes $\bar{\psi}_{0p}(x)$, $p = 1, 2, 3, 4$ drawn as continuous curve and the related natural circular frequency $\bar{\omega}_p$. For comparison the modes of the same beam on elastic foundation are indicated by dashed curve, and the related natural circular frequency is given in brackets. The influence of the elastic foundation is given by the above dimensionless parameter α_1 defined by Eq. (14b). The continuous uniform spring stiffness of the elastic foundation is given by the constant value $\rho_F g b$ in t/m^2 with the specific weight of the fluid (water) $\rho_F g = 1,0$ t/m^3 and the

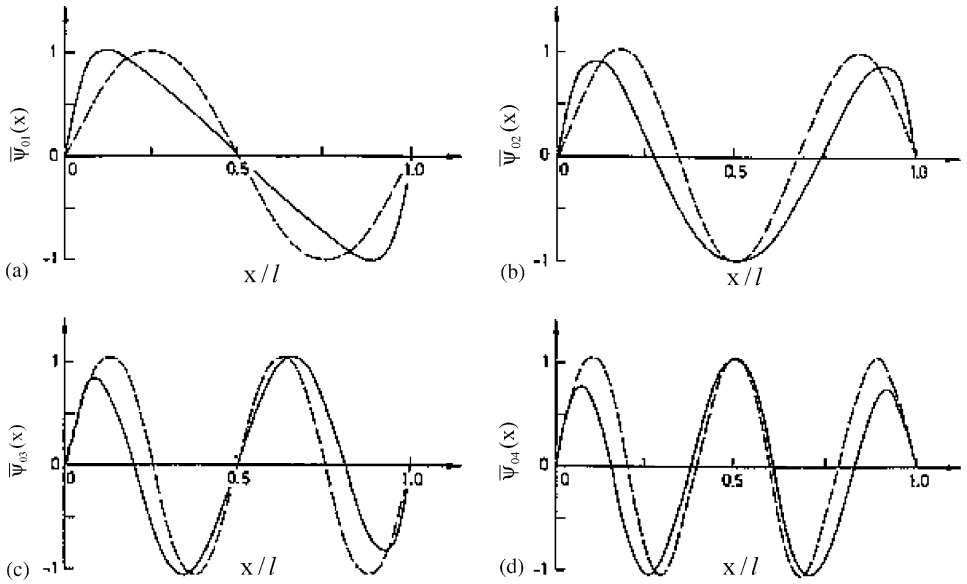

Fig. 3. (a–d) The first four dimensionless beam modes and related natural circular frequencies of the continuous floating bridge chapter 6 as hydroelstic system (——) and as beam on elastic foundation (- - - - -; circular frequencies in brackets). a 1. mode: $\bar{\omega}_1 = 9.3083\,(610.5059)$, b 2. mode: $\bar{\omega}_2 = 18.7182\,(615.6678)$, c 3. mode: $\bar{\omega}_3 = 28.4940\,(629.3568)$, d 4. mode: $\bar{\omega}_4 = 39.2082\,(657.2888)$.

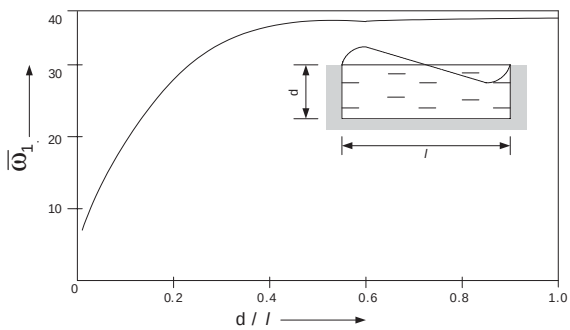

Fig. 4. Dimensionless basic natural circular frequency of the continuous floating bridge chapter 6 versus the proportion of water depth to bridge length.

beam width b in m. Fig. 3 was based on a continuous light weight pontoon bridge made of steel with parameters taken from the example in below chapter 6.

The analysis was carried out using 50 Fourier-coefficients for each beam mode, in order to avoid a gap at both ends of the beam vibrating with symmetric beam modes, which are calculated using Fourier-cosine series, and to get sufficient accuracy for the natural circular frequencies. The basic hydroelastic beam mode $\bar{\psi}_{01}(x)$ is an antimetric curve because of the condition to compensate the displaced incompressible fluid volume. Compared with the beam on elastic foundation the values of natural circular frequency for the hydroelastic beam are essentially smaller and have larger intervals. The reason for the much lower values of the natural circular

frequencies for the hydroelastic vibrating beam compared with those ones of the vibrating beam on elastic foundation is the effect of the dynamically activated fluid mass acting as an added mass to the beam mass. This is also well-known fact in ship building.

If varying water depth d, we get the curve Fig. 4 for the basic related hydroelastic natural circular frequency $\bar{\omega}_1$ versus proportion d/l. According to Fig. 4 the basic hydroelastic natural circular frequency approaches finite upper limit value with increasing water depth. The phenomenon of decreasing hydroelastic natural frequency (or increasing hydrodynamic mass) with decreasing water depth was already noticed by Wendel [28] in connection with bending vibrations of ships in vertical direction. A possible reason for this phenomenon may be the rapid decrease of the vertical component of flow velocity in shallow water simulating a heavy resonating (fluid) mass.

4. Modal analysis of forced hydroelastic vibrations

In the following the hydroelastic beam vibration will be considered under the effect of a single axle vehicle running with uniform speed along the beam. For the $p = 1, 2, \ldots$ beam modes of the homogeneous floating beam the following orthogonal relations exist according to Ref. [27]:

$$\frac{1}{l}\int_0^l \bar{\psi}_{0p}\bar{\psi}_{0q}\mathrm{d}x + \alpha_3\frac{1}{l}\int_0^l \bar{\psi}_{1p}\bar{\psi}_{1q}\,\mathrm{d}x - \alpha_2\frac{1}{l}\int_0^l \bar{\Phi}_p(x,h)\bar{\psi}_{0q}\,\mathrm{d}x := \begin{cases} 0 & \text{for } q \neq p, \\ \bar{M}_p & \text{for } q = p \end{cases} \tag{31a}$$

and

$$\alpha_1\frac{1}{l}\int_0^l \bar{\psi}_{0p}\bar{\psi}_{0q}\,\mathrm{d}x + \frac{1}{l}\int_0^l \bar{\psi}_{2p}\bar{\psi}_{2q}\,\mathrm{d}x := \begin{cases} 0 & \text{for } q \neq p, \\ \bar{M}_p\bar{\omega}_p^2 & \text{for } q = p. \end{cases} \tag{31b}$$

The inhomogeneous partial differential equation (3) of the floating beam shall be solved using the following series approaches:

$$\tilde{w}(x,t) = l\sum_{p=1}^{\infty} Y_p(t)\bar{\psi}_{0p}(x), \tag{32a}$$

$$\Phi(x,z,t) = l^2\sum_{p=1}^{\infty} \dot{Y}_p(t)\bar{\Phi}_p(x,z). \tag{32b}$$

These two approaches are inserted into the differential Eq. (3) using partial differentiation of each term of the series considering definition (12b). After multiplying the resulting equation with $l\bar{\psi}_{0q}(x)$, $q = 1, 2, \ldots$ and integrating each term from $x = 0$ to l under consideration of the orthogonal relations (31) we will get a system of coupled common second order differential equations for the time functions $Y_p(t)$, $p = 1, 2, \ldots$ The differential equations are coupled, because the damping terms are multiplied with the integrals

$$\int_0^l \bar{\psi}_{0p}(x)\bar{\psi}_{0q}(x)\,\mathrm{d}x \quad \text{and} \quad \int_0^l \bar{\psi}_{2p}(x)\bar{\psi}_{2q}(x)\,\mathrm{d}x$$

for $q \neq p$. If we acknowledge the value of integrals over the mixed mode functions ($q \neq p$) as small compared with the value of the integrals over the square of the mode functions ($q = p$), then this

so called comfortable hypothesis will allow the system of differential equations to be de-coupled resulting in $p = 1, 2, \ldots$ independent common differential equations

$$\ddot{Y}_p + \dot{Y}_p \omega_p \bar{R}_p + Y_p \omega_p^2 = \omega_p^2 \bar{f}_p(t), \quad p = 1, 2, \ldots \tag{33}$$

with the dimensionless parameters

$$\bar{R}_p := \frac{\bar{r}_p}{\bar{\omega}_p}, \quad \bar{r}_p = \frac{1}{\bar{M}_p}\left[\frac{\alpha_4}{l}\int_0^l \bar{\psi}_{0p}^2 \,\mathrm{d}x + \frac{\alpha_5}{l}\int_0^l \bar{\psi}_{2p}^2 \,\mathrm{d}x\right], \quad \bar{f}_p(t) = \frac{P(t)}{\bar{M}_p \bar{\omega}_p^2}\frac{\bar{\psi}_{0p}(ct)}{\omega_c^2 \mu_c l^2}$$

and the dimensionless "generalized mass" $\bar{M}_p$ according to Eq. (31a) as well as the definitions

$$\omega_c := \sqrt{\frac{EI}{\mu l^4}}, \quad \alpha_5 := \frac{r_i I}{\mu \omega_c l^4}, \quad \alpha_4 := \frac{r_a}{\mu \omega_c}.$$

Considering the load function from Eq. (8) the solution of the differential equation (33) is the dimensionless time function

$$Y_p(t) = G_{1p}(t) - \int_0^t \ddot{v}_1(\tau) G_{2p}(t, \tau) \,\mathrm{d}\tau, \quad p = 1, 2, \ldots. \tag{34}$$

In Eq. (34) the following two functions are well known:

$$G_{1p}(t) = c_{1p} g_{1p}(t) + c_{2p} g_{2p}(t) + \frac{C}{\bar{M}_p}\int_0^t [c_0 + c_1 g_1(\tau) + c_2 g_2(\tau)]\bar{\psi}_{0p}(c\tau) g_{1p}(t - \tau) \,\mathrm{d}\tau, \tag{35a}$$

where the two products standing before the integral term are the solution for the free vibration, and

$$G_{2p}(t, \tau) = \frac{C}{\bar{M}_p}\left\{ c_3 \bar{\psi}_{0p}(c\tau) g_{1p}(t - \tau) + \int_\tau^t \bar{\psi}_{0p}(c\tau^*) g_{1p}(t - \tau^*)[c_4 g_1(\tau^* - \tau) + c_5 g_2(\tau^* - \tau)] \,\mathrm{d}\tau^* \right\}. \tag{35b}$$

In Eqs. (35a) and (35b) the functions $g_{1p}(t)$, respectively, $g_{2p}(t)$ are equivalent with the functions $g_1(t)$, respectively, $g_2(t)$ of Appendix B, but here have the different meaning

$$\lambda_p^2 := \omega_p^2 - \delta_p^2, \quad p = 1, 2, \ldots \text{ in } \mathrm{s}^{-2}$$

instead of λ_{Fz}^2 and

$$\delta_p := \tfrac{1}{2}\omega_p \bar{R}_p, \quad p = 1, 2, \ldots \text{ in } \mathrm{s}^{-1}$$

instead of δ_{Fz} as well as

$$c_{1p} := \delta_p Y_p(0) + \ddot{Y}_p(0) \text{ in } \mathrm{s}^{-1}, \; c_{2p} := Y_p(0)$$

and

$$C := \frac{1}{\mu l^2} \text{ in } \mathrm{kgf}^{-1}\,\mathrm{s}^{-2}.$$

Each integrand of Eqs (35a) and (35b) has the same common demoninator. In case of zero demoninator the integrals do not exist. This condition is fulfilled, if the vehicle damping reaches the pth damping of beam, i.e.,

$$\delta_p - \delta_{Fz} = 0$$

and if simultaneously the vehicle speed c reaches the critical limit

$$c_{\text{crit}} = \begin{cases} \dfrac{l}{n\pi}\|\lambda_p| \pm |\lambda_{Fz}\|, & \lambda_p^2 \geqslant 0, \quad \lambda_{Fz}^2 \geqslant 0, \\ \dfrac{l}{n\pi}\lambda_p, & \lambda_p^2 > 0 \end{cases} \tag{36}$$

with $p = 1, 3, \ldots$ and $n = 2, 4, \ldots$ from Eq. (15) for antimetric modes or with $p = 2, 4, \ldots$ and $n = 1, 3, \ldots$ from Eq. (29) for symmetric modes. This case is equivalent with resonance under stationary dynamic loading. Vehicle crossings are transient dynamic actions with finite beam deflections also in non-damping case (cf. Ref. [1]).

Using Eq. (36), the following critical vehicle speeds can be calculated for the pontoon bridge discussed in below Chapter 6:

p	n	c_{crit} in km/h
1	2	9.7
2	1	39.0
3	2	29.7
4	1	81.7

5. Acceleration and course of wheel load

The vertical movement $v_1(t)$ of the wheel axle respectively of the wheel load $P(t)$ at the momentary station $x_1(t) = ct$ is according to Fig. 5 equivalent with the summation of

- the static beam deflection $\bar{w}_1(t) \coloneqq \bar{w}_1(x_1(t))$ due to dead load,
- the dynamic beam oscillation $\tilde{w}_1(t) \coloneqq \tilde{w}(x_1(t), t)$ around the static beam deflection and
- the track unevenness $u_1(t) \coloneqq u(x_1(t))$,

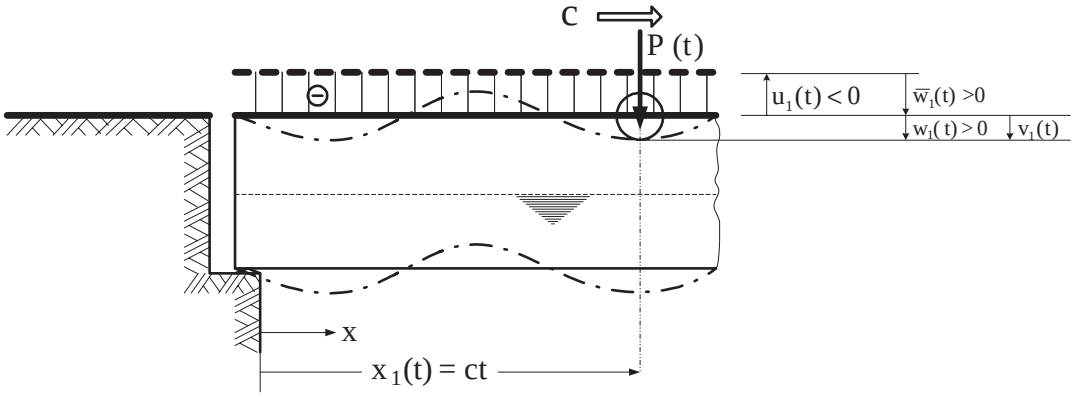

Fig. 5. - - - track level in case of weightless beam including surface roughness. —— track level in case of beam with dead load including surface roughness. $\tilde{w}(x, t)$ = dynamic beam deflection (oscillation) due to traffic. $\bar{w}(x)$ = static beam deflection due to dead load. ||||||| $u(x)$ = track un-evenness.

i.e.,

$$v_1(t) = \bar{w}_1(t) + \tilde{w}_1(t) + u_1(t).$$

The track unevenness $u(x)$ shall be defined here as the distance between the bank level ($u = 0$) and the track contour including surface roughness of the weightless floating beam at rest (downward direction $u > 0$). After the static beam deflection $\bar{w}(x)$ has occurred due to dead load and the ends of floating beam have been fixed on the banks, the track is assumed to have same height with bank level (no step). From above summation formula it is derived

$$\tilde{w}_1(t) = v_1(t) - \bar{w}_1(t) - u_1(t). \tag{37}$$

Inserting expression (37) of the dynamic beam oscillation into the left side of Eq. (32a) describing the dynamic response of the vibrating beam at the momentary load station $x_1(t) = ct$ and considering expression (34) of time function will result in the following integro-differential equation for the course $v_1(t)$ of the wheel load:

$$\frac{v_1(t)}{l} = \frac{\bar{w}_1(t)}{l} + \frac{u_1(t)}{l} + \sum_{p=1}^{\infty}\left[G_{1p}(t)\bar{\psi}_{0p}(ct) - \int_0^t \ddot{v}_1(\tau)\sum_{p=1}^{\infty} G_{2p}(t,\tau)\bar{\psi}_{0p}(ct)\,\mathrm{d}\tau\right]. \tag{38}$$

According to [29] Eq. (38) can be replaced by two integral equations, from which one after another the (vertical) acceleration of wheel load $\ddot{v}_1(t)$ and then the (vertical) course of wheel load $v_1(t)$ can be determined at any moment (see also Ref. [27]).

The acceleration of wheel load is part of the following first degree Volterra type integral equation:

$$\int_0^{\bar{t}} \Gamma(\bar{t},\bar{\tau})\bar{F}(\bar{\tau})\,\mathrm{d}\bar{\tau} = R(\bar{t}), \quad 0 \leqslant \bar{t} \leqslant 1 \tag{39}$$

with the kernel

$$\Gamma(\bar{t},\bar{\tau}) = \bar{t} - \bar{\tau} + \sum_{p=1}^{\infty} \bar{G}_{2p}(\bar{t},\bar{\tau})\bar{\psi}_{0p}(ct(\bar{t}))$$

and the right side

$$R(\bar{t}) = -\alpha_{12}^2(\alpha_6 + \alpha_7\bar{t}) + \alpha_{12}^2\left(\frac{\bar{w}_1(t(\bar{t}))}{l} + \frac{u_1(t(\bar{t}))}{l}\right) + \sum_{p=1}^{\infty} \bar{G}_{1p}(\bar{t})\bar{\psi}_{0p}(ct(\bar{t}))$$

using the definitions

$$\bar{t} \coloneqq \Omega t, \quad \Omega \coloneqq \frac{c}{l} \text{ in } \mathrm{s}^{-1}, \quad \bar{F}(v) \coloneqq \frac{\ddot{v}_1(\tau(\bar{\tau}))}{g},$$

$$\bar{G}_{1p}(\bar{t}) \coloneqq \alpha_{12}^2 G_{1p}(t(\bar{t})), \quad \bar{G}_{2p}(\bar{t},\bar{\tau}) \coloneqq \alpha_{12}^2\frac{g}{\Omega}G_{2p}(t(\bar{t}),\tau(\bar{\tau})),$$

$$\alpha_6 \coloneqq \frac{v_1(0)}{l}, \quad \alpha_7 \coloneqq \frac{\dot{v}_1(0)}{l\Omega}, \quad \alpha_{12} \coloneqq \Omega\sqrt{\frac{l}{g}}.$$

If the total passage time of the vehicle is divided into constant time steps, the integral equation (39) leads to a recursion formula, from which the wheel load acceleration can be calculated at any

moment of passage. From a second integral equation

$$\frac{v_1(t(\bar{t}))}{l} = \frac{1}{\alpha_{12}^2}\int_0^{\bar{t}} (\bar{t}-\bar{\tau})\bar{F}(\bar{\tau})\,\mathrm{d}\bar{\tau} + \alpha_6 + \alpha_7\bar{t}, \quad 0 \leqslant \bar{t} \leqslant 1 \tag{40}$$

the course of wheel load can be derived time step by time step using the solution of Eq. (39). According to Eq. (34) the acceleration of wheel load governs the time function $Y_p(t)$ and the state of the coupled hydroelastic system of fluid–beam–vehicle. Based on the above algorithms the author developed a computer program, which is attached in Ref. [27]. The integrals within functions (35a) and (35b) were solved by analytical methods.

6. Example

Analysis results shall be shown for a realistic floating bridge made of continuous steel plates with hollow cross-section fully covering the fluid surface of a rectangular water filled basin hinged to the bridge ends. Hydroelastic effects transverse bridges are neglected (rigid cross-section). Therefore, hydrodynamic damping effects due to lateral wave radiation cannot occur (worst case). Internal and external material damping will be neglected. The vehicle is simulated by an unsprung single mass passing the bridge with uniform speed along the centerline of the bridge from the left bank to the right bank.

The system parameters according to Fig. 1 are given below as follows:

$$l = 150\,\mathrm{m}, \quad b = 7.30\,\mathrm{m}, \quad d = 2.80\,\mathrm{m}, \quad E = 2,100\,\mathrm{t/cm^2}, \quad I = 47.414 \times 10^{-5}\,\mathrm{m^4},$$
$$\mu = 0.134\,\mathrm{t\,s^2/m^2}, \quad \rho_F g = 1.0\,\mathrm{t/m^3}, \quad r_i = 0, \quad r_a = 0.$$

The vehicle parameters according to Fig. 2 are given below as follows:

$$c = 20\,\mathrm{km/h}, \quad m_1 = 4.852\,\mathrm{t\,s^2/m}, \quad m_2 = 0, \quad c_{Fz} = 0, \quad r_{Fz} = 0.$$

The related dimensionless parameters α_1, α_2 and α_3 according to Eq. (14b) are given with Eq. (31). Fig. 3 shows the beam modes and natural circular frequencies of this floating bridge. Fig. 4 shows the course of the related basic natural circular frequency of this bridge versus varying water depth.

The track is assumed smooth and horizontal, so that for the course of wheel load the expression $\bar{w}_1(t) + u_1(t)$ in Eq. (38) is zero (cf. Fig. 5).

Fig. 6(a) shows the related course of wheel load, v_1/l, versus the related load position x/l using a continuously drawn curve. Also the related beam deflection curve $\tilde{w}_1/l$ versus the related load position x/l is shown for the load positioned at mid-span ($\bar{t} := t \cdot c/l = 0.5$) using dashed line and beyond mid-span a little moment later ($\bar{t} = 0.51$) using combined dashed-dotted line. Each position of the wheel load is marked by a circle on the continuously drawn line v_1/l. The wheel runs along a curve, which characteristically starts oscillating with high amplitudes when the wheel is approaching mid-span; afterwards the wheel will be even uplifted above the static bridge level shortly before reaching the opposite bank. This phenomenon can be explained by quasi-resonant behavior of the system, because here the applied vehicle speed $c = 20\,\mathrm{km/h}$ lies between the basic and the second critical speed of the system (see table below Eq. (36)). Indeed, this phenomenon

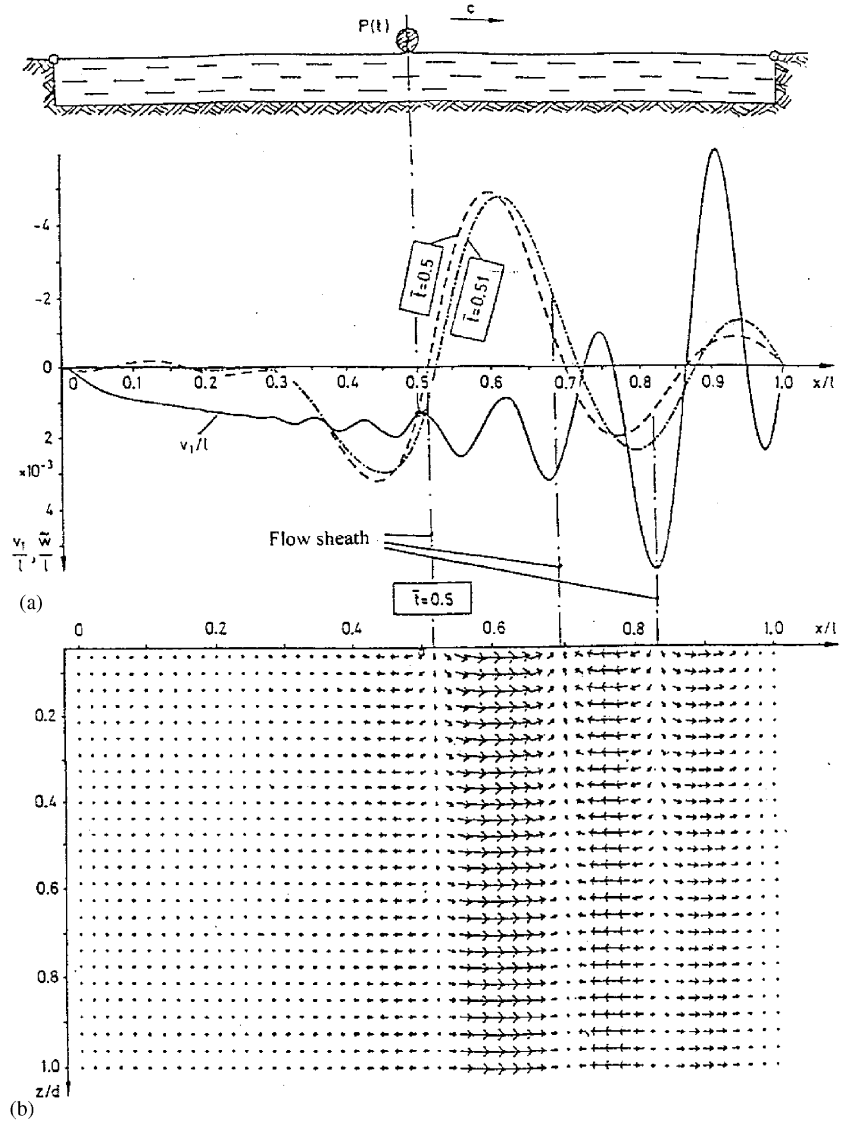

Fig. 6. (a,b) Dynamic state of floating bridge during passage by uniformly moving single mass. (a) course of wheel load (——) and momentary beam deflection curve at time $\bar{t} = 0.5$ (- - -) and $\bar{t} = 0.51$(– · – · –) (b) Flow velocity vectors within the whole fluid at time $\bar{t} = 0.5$.

also can be watched in reality during passage of a heavy vehicle running on deck of a light weight pontoon bridge with certain speed.

According to definition, the momentary dynamic beam deflection curve coincides with the surface waves of the sloshing fluid. The shift of beam deflection curves alias surface waves shown in Fig. 6(a) within the considered time step indicates surface waves of progressing type near mid-span and those ones of standing type near the supports. The nature of surface waves determines the water flow. Fig. 6(b) shows the vector field of flow velocity within the whole fluid area, when

the load reaches at mid-span, i.e., the streamlines at half the passage. It can be clearly seen, how the water is going to flow into hollow parts caused by the progressing beam deflection curve.

The fluid flow here resembles the situation in case of gravity waves with free surface (cf. Ref. [30]): The water volume is divided into several columns along the beam, which are separated from each other by a vertical flow sheath. The flow within one such column occurs more or less in horizontal direction, i.e., parallel the bottom of water bed, and is sharply diverted into vertical direction close to the flow sheath (cf. Ref. [31]).

Fleischer [27] made an estimation on the impact of the non-linear term of fluid pressure $\rho_F v^2/2$ in Eq. (2) using the fluid velocities, which result from the linear theory. This estimation shows, that compared with the linear fluid pressure the effect of non-linear fluid pressure can be neglected behind the vehicle, but in front of the vehicle the non-linear fluid pressure partially can reach the magnitude of the linear fluid pressure and thus should be considered there. This statement is valid especially, if the uniform vehicle speed c lies within a certain range depending on the system parameters. For vehicle speeds outside this range the application of the linear theory is deemed sufficient in the whole region.

7. Case studies

Fig. 7 shows the impact of parameter variations on the course of wheel load, v_1/l, and the momentary dynamic beam deflection curve, when the vehicle reaches at mid-span ($\bar{t} = 0.5$), and short time later ($\bar{t} = 0.51$). Only one parameter will be changed each, all others will be kept same as chosen in above chapter 6, respectively Fig. 6.

Fig. 7(a) is based on applying an extremely low vehicle speed $c = 0.001$ km/h equivalent to quasi-static passage. The course of wheel load as well as the momentary beam deflection curve show characteristic reactions of a beam on elastic foundation. The strange upward convexity of the beam deflection curve above the static bridge level is caused by the compensation condition according to Eq. (7), as the water surface shall be fully covered by the bridge deck.

Fig. 7(b) is based on applying the vehicle speed $c = 40$ km/h, which practically can be deemed maximum speed to safely cross long light weight pontoon bridges. As this vehicle speed is close to the (second) critical speed 39.0 km/h (see table below Eq. (36)), the bridge shows resonant effects during vehicle passage, which are more severe than for half the speed as used in case of Fig. 6. Compared with Fig. 6(a), there are larger number of up and downs of the vehicle course as well as of the beam deflection curve with more peaks above static bridge level especially during the second half of the passage, but obviously having lower amplitudes.

Fig. 7(c) is based on the water depth $d = 50$ m, which is more than 17 times the depth in case of Fig. 6. Here, the type of passage is much more balanced than in case of Fig. 6(a): The course of the vehicle stays below the static bridge level (like in the quasi-static case Fig. 7(a)) and the up and downs of the curves are moderate. This obviously less severe dynamic response of the concerned floating bridge on deep water ($d = 50$ m) compared with that one on shallow water ($d = 2.80$ m) can be explained by non-resonant behavior of the system. According to Fig. 4 and Eq. (36) the basic critical vehicle speed here is 35.7 km/h, which is 1.78 times higher than the applied one 20 km/h.

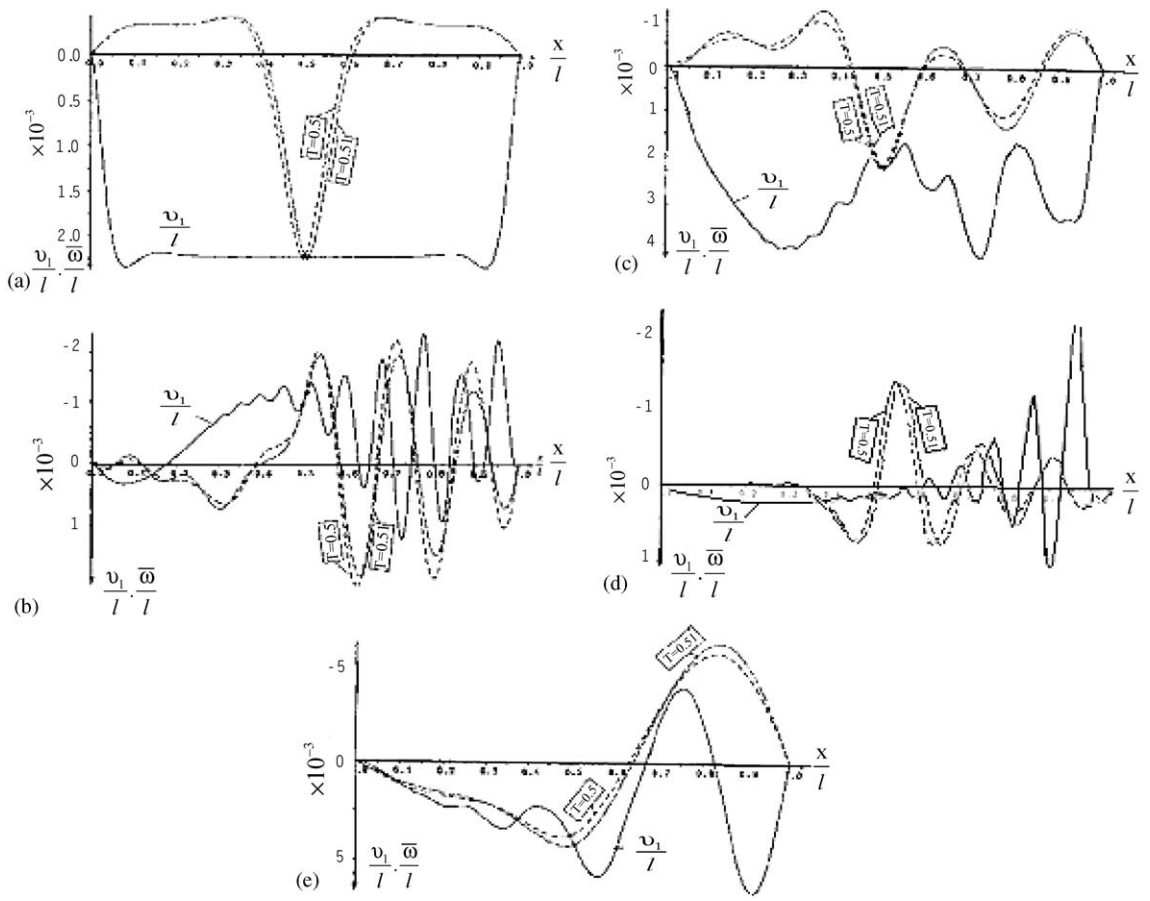

Fig. 7. Course of wheel load v_1/l (——) and momentary beam deflection curve at time $\bar{t} = 0.5$ (- - -) and $\bar{t} = 0.51$(– · – · –) of floating bridge during passage by uniformly moving single mass for different parameters: (a) speed $c = 0.001$ km/h; (b) speed $c = 40$ km/h; (c) water depth $d = 50$ m; (d) moment of area $I = 4.7414 \times 10^{-5}$; (e) bridge length $l = 50$ m.

Fig. 7(d) is based on a reduced beam stiffness compared with the case of Fig. 6, that can occur due to tolerances in the connecting parts of the bridge deck elements. Here, the extreme reduction by 90% of the original stiffness is considered. The result is a vehicle course and beam deflection curve similar to Fig. 6(a), but obviously having lower amplitudes.

Fig. 7(e) is based on a bridge with length $l = 50$ m, which is only one third of the bridge length in the case of Fig. 6. The result is a vehicle course and beam deflection curve similar to Fig. 6(a) with trend for smaller amplitudes and a huge bow wave in front of the vehicle bending the beam arch like up to the opposite bank.

8. Summary

The coupled problem of fluid–beam–vehicle interaction is investigated considering the linear potential theory of fluids and is solved for plane fluid flow using modal analysis. The analyzed

example and case studies show the characteristics of dynamic response of the considered hydroelastic system. Also limits of the applied linear theory are indicated.

Appendix A

Explanation and derivation of Eq. (3):

In the following all dynamic internal forces and deformations of the beam element are marked with the $\sim$ symbol:

a) Dynamic loading and reactions on beam element

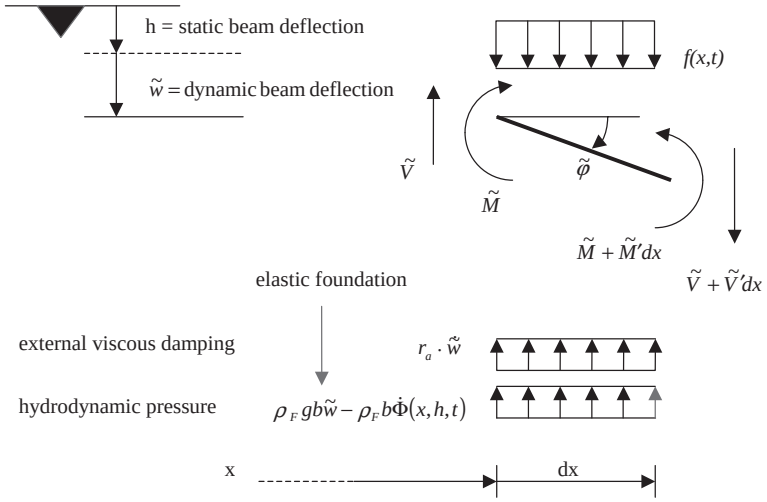

b) Beam fiber model and dynamic bending moment

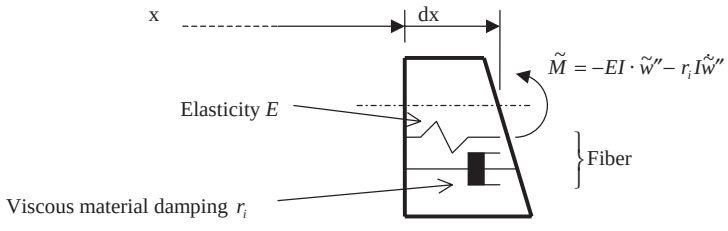

c) Dynamic equilibrium of beam element

For simplicity, the following definitions on symbolizing partial differentiation will be introduced:

$$\dot{\tilde{w}} := \frac{\partial \tilde{w}}{\partial t}, \quad \dot{\Phi} := \frac{\partial \Phi}{\partial t}, \quad \tilde{w}' := \frac{\partial \tilde{w}}{\partial x}. \tag{A.1}$$

Higher partial differentials will be treated in analogous manner.

The sum of forces in vertical direction is according to above sketch (a)

$$\mu\ddot{\tilde{w}}\,\mathrm{d}x = \tilde{V}'\,\mathrm{d}x - r_a\dot{\tilde{w}}\,\mathrm{d}x - \rho_F g b\tilde{w}\,\mathrm{d}x + \rho_F b\dot{\Phi}(x,h,t)\,\mathrm{d}x + f(x,t)\,\mathrm{d}x$$

and after deleting dx

$$\mu\ddot{\tilde{w}} = \tilde{V}' - r_a\dot{\tilde{w}} - \rho_F g b\tilde{w} + \rho_F b\dot{\Phi}(x,h,t) + f(x,t). \tag{A.2}$$

The sum of moments is according to above sketch (a) if neglecting terms with squares of dx

$$\rho I\ddot{\tilde{\varphi}}\,\mathrm{d}x = -\tilde{M}'\mathrm{d}x + \tilde{V}\,\mathrm{d}x$$

and with term for $\tilde{M}$ from above sketch (b) after deleting dx

$$\rho I\ddot{\tilde{\varphi}} = EI\tilde{w}''' + r_i I\dot{\tilde{w}}''' + \tilde{V}. \tag{A.3}$$

From Eq. (A.3) it follows:

$$\tilde{V}' = \rho I\ddot{\tilde{\varphi}}' - EI\tilde{w}'''' - r_i I\dot{\tilde{w}}''''. \tag{A.4}$$

Inserting Eq. (A.4) into Eq. (A.2) will give

$$\mu\ddot{\tilde{w}} = \rho I\ddot{\tilde{\varphi}}' - EI\tilde{w}'''' - r_i I\dot{\tilde{w}}'''' - r_a\dot{\tilde{w}} - \rho_F g b\tilde{w} + \rho_F b\dot{\Phi}(x,h,t) + f(x,t).$$

Resolving this equation to the external continuous load function $f(x,t)$ on the right-hand side and considering the relation

$$\tilde{\varphi}' = \tilde{w}''$$

will result into

$$\mu\ddot{\tilde{w}} - \rho I\ddot{\tilde{w}}'' + \rho_F g b\tilde{w} - \rho_F b\dot{\Phi}(x,h,t) + EI\tilde{w}'''' + r_a\dot{\tilde{w}} + r_i I\dot{\tilde{w}}'''' = f(x,t). \tag{A.5}$$

If in Eq. (A.5) the partial differentials will be substituted by the symbols according to above definitions (A.1), and if the continuous load function on the right-hand side shall describe the time dependant discrete contact force $P(t)$ of a single axle vehicle running with constant velocity c using Dirac's function $\ddot{a}$ (see Ref. [1, p. 14]):

$$f(x,t) = \delta(x - ct)P(t)$$

it will give the partial differential Eq. (3) of Chapter 2

$$\mu\frac{\partial^2\tilde{w}(x,t)}{\partial t^2} - \rho I\frac{\partial^2}{\partial t^2}\left(\frac{\partial^2\tilde{w}(x,t)}{\partial x^2}\right) + \rho_F g b\tilde{w}(x,t) - \rho_F b\frac{\partial\Phi(x,h,t)}{\partial t}$$
$$+ EI\frac{\partial^4\tilde{w}(x,t)}{\partial x^4} + r_a\frac{\partial\tilde{w}(x,t)}{\partial t} + r_i I\frac{\partial}{\partial t}\left(\frac{\partial^4\tilde{w}(x,t)}{\partial x^4}\right) = \delta(x - ct)P(t). \tag{A.6}$$

Appendix B

Related to Eq. (8) and Fig. 2:

$$K_0 = (m_1 + m_2)g \text{ in kgf},$$

$$K_1 = c_{Fz}\left(1 + \frac{m_1}{m_2}\right) = \omega_{Fz}^2(m_1 + m_2) \text{ in kgf m}^{-1},$$

$$K_2 = r_{Fz}\left(1 + \frac{m_1}{m_2}\right) = 2\delta_{Fz}(m_1 + m_2) \text{ in kgf m}^{-1}\text{ s},$$

$$K_3 = m_1 \text{ in kgf m}^{-1}\text{ s}^2,$$

$$\delta_{Fz} = \frac{r_{Fz}}{2m_2} \text{ in s}^{-1} \text{ (damping constant)},$$

$$\omega_{Fz}^2 = \frac{c_{Fz}}{m_2} \text{ in s}^{-2} \text{ (natural circular frequency)},$$

$$\lambda_{Fz}^2 := \omega_{Fz}^2 - \delta_{Fz}^2 \text{ in s}^{-2} \text{ (natural circular frequency of the damped system)},$$

$$c_0 = K_0 \text{ in kgf},$$

$$c_1 = [K_1\delta_{Fz} + (K_3\delta_{Fz} - K_2)\omega_{Fz}^2]y(0) + c_4\dot{y}(0) \text{ in kgf s}^{-1},$$

$$c_2 = (K_1 - K_3\omega_{Fz}^2)y(0) + c_5\dot{y}(0) \text{ in kgf},$$

$$c_3 = K_3 \text{ in kgf m}^{-1}\text{ s}^2,$$

$$c_4 = K_1 - K_2\delta_{\mathrm{Fz}} + K_3(2\delta_{\mathrm{Fz}}^2 - \omega_{Fz}^2) \text{ in kgf m}^{-1},$$

$$c_5 = K_2 - 2K_3\delta_{\mathrm{Fz}} \text{ in kgf m}^{-1}\text{ s},$$

$$g_1(t) = \frac{\sin\lambda_{\mathrm{Fz}}t}{\lambda_{Fz}}\mathrm{e}^{-\delta_{Fz}t} \text{ in s}, \quad g_2(t) = \mathrm{e}^{-\delta_{Fz}t}\cos\lambda_{\mathrm{Fz}}t \quad \text{for } \lambda_{Fz}^2 > 0,$$

$$g_1(t) = \frac{\sinh|\lambda_{\mathrm{Fz}}|t}{|\lambda_{\mathrm{Fz}}|}\mathrm{e}^{-\delta_{Fz}t} \text{ in s}, \quad g_2(t) = \mathrm{e}^{-\delta_{Fz}t}\cosh|\lambda_{\mathrm{Fz}}|t \text{ for } \lambda_{Fz}^2 < 0,$$

$$g_1(t) = t\mathrm{e}^{-\delta_{Fz}t} \text{ in s}, \; g_2(t) = \mathrm{e}^{-\delta_{Fz}t} \quad \text{for } \lambda_{Fz}^2 = 0.$$

References

[1] L. Fryba, *Vibrations of Solids and Structures Under Moving Loads*, Noordhoff Int. Publ., Groningen, 1972.

[2] G.G. Stokes, Discussion of a differential equation relating to the breaking of railway bridges, *Transactions of the Cambridge Philosophical Society* 8 (1849) 707–735.

[3] H. Zimmermann, Die Schwingungen eines Traegers mit bewegter Last, *Centralblatt der Bauverwaltung* 16 (1896) 249–251, 257–260, 264–266.

[4] A. Schallenkamp, Schwingungen von Traegern bei bewegten Lasten, *Ingenieur Archiv* 8 (1937) 182–188.

[5] E. Marquard, Zur Berechnung von Brueckenschwingungen unter rollenden Lasten, *Ingenieur Archiv* 23 (1955) 19–35.

[6] K.G. Schuetz, Untersuchung des gekoppelten Schwingungssystems Bruecke-Fahrzeug-Tilger unter besonderer Berueckksichtigung von Fahrbahnunebenheiten, Diss. TU Muenchen 1988, Mitteilungen aus dem Lehrstuhl fuer Stahlbau Heft 24.

[7] St. Drosner, Beitrag zur Berechnung der dynamischen Beanspruchung von Bruecken unter Verkehrslasten, Diss. RWTH Aachen 1989, Schriftenreihe Stahlbau RWTH Aachen Heft 16.
[8] Chr. Petersen, Optimierung militaerischer Pontonbruecken aus historischer Sicht. In: H.R. Beierlein, D. Koenke (Eds.), *Tagungsband internationales wehrtechnisches Symposium "Militaerische Bruecken"*, Maerz 1990, BMVgRueIII5, Bonn, pp. 237–260.
[9] A. Brekken, Pongtongbroer, *Teknisk Ukeblad* 108 (1961) 257–261.
[10] R.W. Gaul, Hood canal bridge, *Civil Engineering* 32 (1962) 40–43.
[11] B.J. Hartz, Dynamic analysis of the Hood Canal floating bridge failure, in: *Proceedings of the ICOSSAR' 81*, Amsterdam, Elsevier, Oxford, New York 1981, pp. 545–557.
[12] J.H. Vugts, The hydrodynamic coefficients for swaying, heaving and rolling cylinders in a free surface, *International Shipbuilding Progress* 15 (1968) 251–276.
[13] I. Holand, I. Langen, Salhus floating bridge, Progress Report No. 2: Theory, hydrodynamic coefficients, SINTEF Report, November 15, 1972.
[14] R.E.D. Bishop, W.G. Price, *Hydroelasticity of Ships*, Cambridge University Press, Cambridge, 1979.
[15] I. Langen, Probabilistic methods for dynamic analysis of floating bridges, *Norwegian Maritime Research* 1 (1983) 2–15.
[16] C. Georgiadis, CGFLOAT, a computer program for the dynamic analysis of floating bridges and breakwaters, *Advances in Engineering Software* 5 (1983) 215–220.
[17] M. Myint Lwin, Design of the third Lake Washington floating bridge, *Concrete International* 11 (1989) 50–53.
[18] F. Rischbieter, Das Zellenmodell und seine Adaptierung zur dynamischen Untersuchung kontinuierlich gestuetzter Schwimmbruecken, in: *Bericht ueber das Symposium vom 9. und 10. Maerz 76 "Sonderprobleme militaerischer Bruecken und Uebersetzmittel"*, T2.2-10.01 bis 14 und T2.2-10.B1/1 bis B8/9, Bundesakademie fuer Wehrverwaltung und Wehrtechnik Dez, Mannheim, 1976.
[19] S. Chonan, Moving load on a pre-stressed plate resting on a half space, *Ingenieur Archiv* 45 (1976) 171–178.
[20] J.W. Davys, R.J. Hosking, A.D. Sneyd, Waves due to a steadily moving source on a floating ice plate, *Journal of Fluid Mechanics* 158 (1985) 269–287.
[21] R.M.S.M. Schulkes, R.J. Hosking, A.D. Sneyd, Waves due to a steadily moving source on a floating ice plate, Part 2, *Journal of Fluid Mechanics* 180 (1987) 297–318.
[22] R.M.S.M. Schulkes, A.D. Sneyd, Time-dependant response of floating ice to a steadily moving load, *Journal of Fluid Mechanics* 186 (1988) 25–46.
[23] H. Lamb, On the vibrations of an elastic plate in contact with water, *Proceedings of the Royal Society of London A* 98 (1921) 205–216.
[24] O. Grim, Hydrodynamische Traegheits- und Daempfungskraefte, hydrodynamische schwingungserregende Kraefte, Kontakt-Studium, 8, Fortbildungskurs, Institut fuer Schiffbau der Universitaet Hamburg, Okt, 1975.
[25] H.F. Bauer, Hydroelastic vibrations in a rectangular container, *International Journal of Solids and Structures* 17 (1981) 639–652.
[26] H.F. Bauer, W. Eidel, Non-linear hydroelastic vibrations in rectangular containers, *Journal of Sound and Vibration* 125 (1988) 93–114.
[27] Fleischer, D., Analytische Berechnung der linearen, hydroelastischen Schwingungen eines schwimmenden Rechteckbalkens unter einem gleichfoermig bewegten Einachsfahrzeug bei ebener Potentialstroemung des Fluids, Diss. Universitaet der Bundeswehr Muenchen, 1991, Lehrstuhl fuer Stahlbau Heft Nr.9/91.
[28] K. Wendel, Hydrodynamische Massen und hydrodynamische Massentraegheitsmomente, *Jahrbuch der Schiffbautechnischen Gesellschaft Bd.* 44 (1950) 207–255.
[29] M.Y. Ryazanova, On beam vibrations under the effect of a load moving along it (Russian), *Dopovidi Akademii Nauk Ukrains'koi RSR* 20 (2) (1958) 157–161.
[30] O. Tietjens, *Stroemungslehre, Physikalische Grundlagen vom technischen Standpunkt, Erster Band: Hydro- und Aerostatik, Bewegung der idealen Fluessigkeit*, Springer, Berlin, Goettingen, Heidelberg, 1960.
[31] A. Sommerfeld, *Vorlesungen ueber Theoretische Physik Band II: Mechanik der deformierbaren Medien*, Akademische Verlagsanstalt Geest & Portig K.G., Leipzig, 1964.